Radar Systems and
Remote Sensing Laboratory





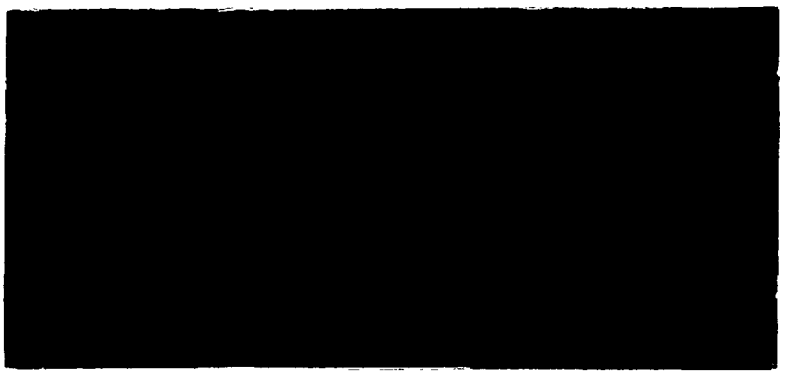



THE UNIVERSITY OF KANSAS CENTER FOR RESEARCH, INC.
2291 Irving Hill Road
Lawrence, Kansas 66045-2969

# SCAN PATTERNS AND ACCURACY OF A RADAR WIND SENSOR (RAWS)

S. Song, B. Beh, and R. K. Moore

Radar Systems and Remote Sensing Laboratory
Department of Electrical Engineering and Computer Science, University of Kansas
2291 Irving Hill Road, Lawrence, Kansas 66045-2969
TEL: 913/864-4835 * FAX: 913/864-7789 * E-MAIL: graham@ardneh.rsl.ukans.edu

RSL Technical Report 11170-2

November 1995

Sponsored by:

NASA Marshall Space Flight Center
MSFC, AL 35812

Grant No. NAG8-1095

# SCAN PATTERNS AND ACCURACY OF A RADAR WIND SENSOR (RAWS)

Shuxian Song, Beng Beh, and Richard K. Moore
Radar Systems and Remote Sensing Laboratory
The University of Kansas
2291 Irving Hill Road
Lawrence KS 66045-2969

## ABSTRACT

The Radar Wind Sensor (RAWS) was proposed as a complement to laser wind sensors, allowing coverage in cloudy regions excluded from laser coverage. Previous University of Kansas studies showed the feasibility of the wind measurement at various levels in the atmosphere and indicated that RAWS can also measure rain rates and ocean-surface winds. Here we discuss measurement of the wind vector in terms of the scan patterns for a conically scanned antenna. By using many measurements from cells about 66 km square and 132 km square, a least-squares algorithm gives results that are reasonable for insertion into global atmospheric models. For RAWS to be used successfully as a complement to a laser wind sensor, the design of the two sensors should be integrated and radial velocity measurements in a given atmospheric cell should be combined to get the most accurate results.

# Introduction

Modeling global atmospheric circulations and forecasting the weather would improve greatly if worldwide information on winds aloft were available. Recognition of this led to the inclusion of the Laser Wind Sounder (LAWS) to measure Doppler shifts from aerosols in the original plan for Earth Observation System (EOS) [1]. However, gaps would exist in LAWS coverage where clouds are present. The RAdar Wind Sensor (RAWS) was proposed to fill these gaps by measuring Doppler shifts from clouds and rain [2,3].

Previous studies showed that RAWS is technologically feasible. Sensitivity studies showed the best single frequency and pairs of frequencies [4] and the required antenna size. With the original power proposed, RAWS could measure most clouds types. With reduced power, it can measure all but thin clouds [5]. The conical scan pattern gives two looks for every point measured [2]. Use of estimates of the raindrop fall speed based on rain-echo intensity solved the problem of the dependence of the wind solution on the vertical speed of hydrometeors [6]. Also, studies showed that the combination of a laser and a microwave radar would reduce the power requirements of the microwave radar [7].

This report discusses the derivation of the true wind velocity from multiple measurements of radial velocity. Ideally the conical scan pattern would provide intersections of forward- and aft-looking radial velocity measurements for individual points. In fact, the forward motion during conical scans is such that one must use measurements from nearby, but not coincident, points for most of the coverage area. In this report, we show simulations that indicate the accuracies that may be achieved by using all measurements within a particular grid square.

# Antenna Scan Pattern and Measured Points

RAWS uses a conical scan pattern that is similar to the proposed LAWS scan pattern. The scan method is shown in Fig. 1. There, h is the altitude of the radar and θ the nadir angle

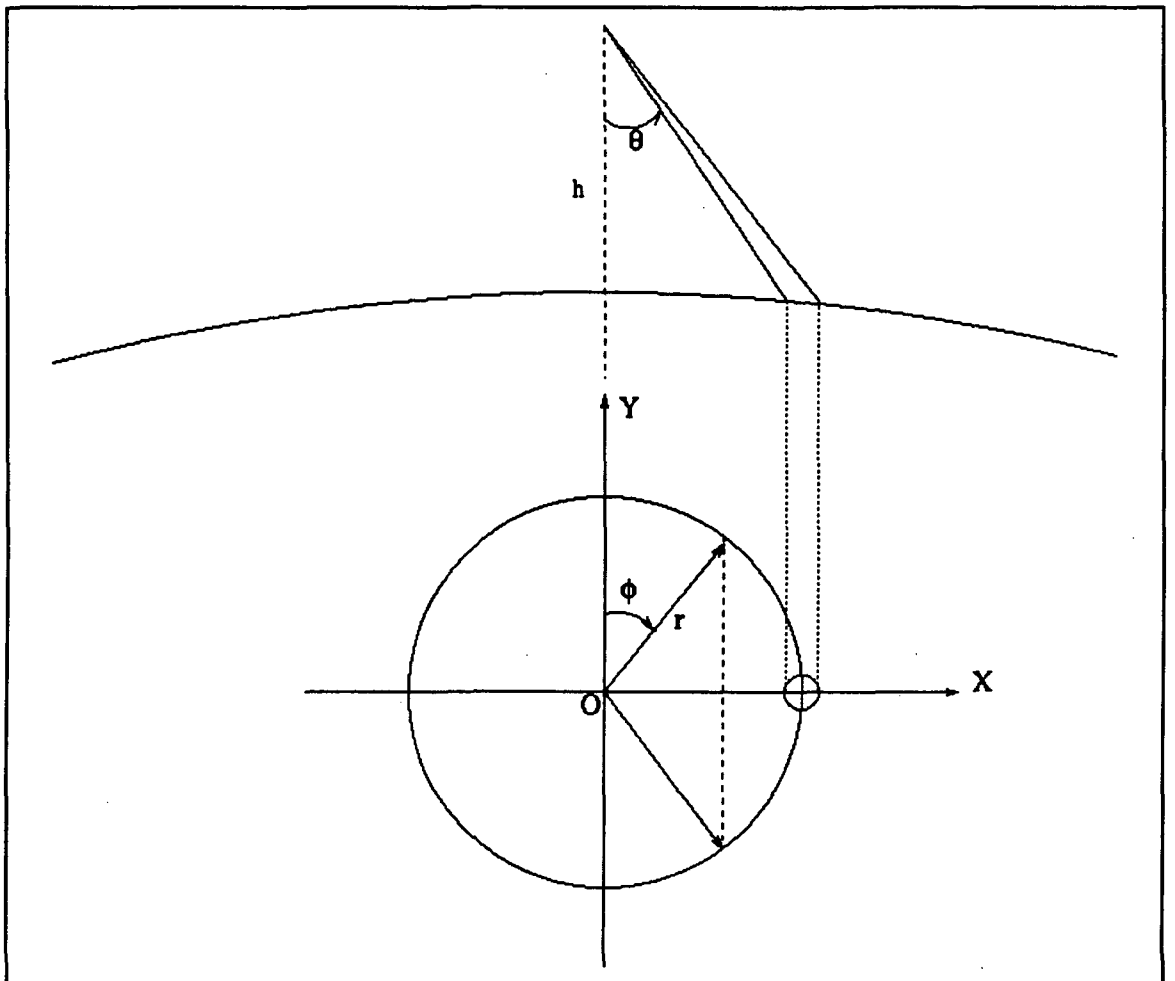


Fig. 1. Conical scan pattern for RAWS.

of the scan beam. This is a single-beam scan that allows two looks at a given area along the path parallel to the antenna moving velocity vector. The scan paths on the ground are plotted in Fig. 2.

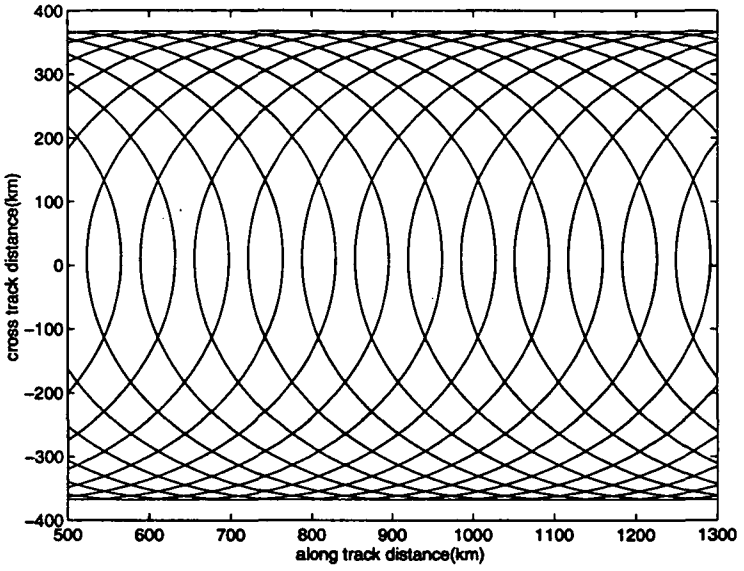


Fig. 2. RAWS scan paths on the ground.

The possible scan swath width using plane geometry is

$$W=2h\cdot\tan(\theta) \tag{1}$$

When the radius of the Earth is considered, W becomes

$$W_{arc}=a(\theta_2-\theta) \tag{2}$$

where a is the radius of the Earth and $\theta_2$ is

$$\theta_2=\sin^{-1}\left(\frac{h+a}{a}\sin\theta\right) \tag{3}$$

The possible measured points on the scan path depend on the scan period $T_p$ and the antenna dwelling time $t_d$ at one point. The total number of points on one scan circle is

$$n = \frac{T_p}{t_d} \tag{4}$$

where $T_p$ depends on the measurement accuracy requirements and is chosen to be $T_p$ = 10s [2]. The look time at one point depends on the number of pulses used for each look and the pulse period T. For transmission of pulse pairs [5], T is calculated as 207.8μs. Table 1 shows the scan parameters for a different number of pulses averaged per point. Using more pulses per point

**Table 1. Scan Parameters for Different Pulses per Point**

| Pulses per Point | 128 | 256 | 512 | 1024 |
|---|---|---|---|---|
| Distance between Points (km) | 6.14 | 12.28 | 24.57 | 49.14 |
| Change of the Azimuth Angle (Degree) | 0.027 | 0.055 | 0.110 | 0.220 |
| Distance Antenna Moved (km) | 0.176 | 0.351 | 0.702 | 1.404 |

increases the angles and the distances between two points.

The distribution of measured points near the surface is shown in Fig. 3, where the asterisks are the forward looks and the circles are the aft looks. From the figure, we see that the distribution is not uniform. Measurements in the edge area are much more dense than in the center area. This influences the wind solution from the data measured at these areas.

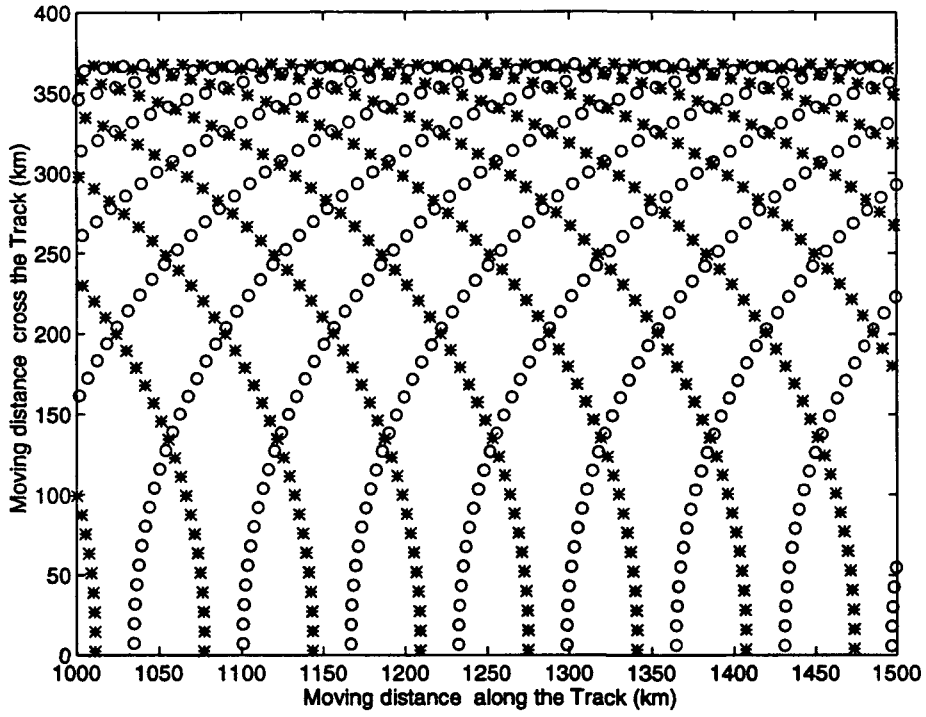


Fig. 3. Measured points on the ground.

# Derivation of the Wind Velocity from the Measured Doppler Velocity

Let the true wind velocity be

$$\overline{U_w} = U_{wx}\overline{x} + U_{wy}\overline{y} + U_{wz}\overline{z} \tag{5}$$

where the z-direction component $U_{wz}$ is derived from the rain fall speed [6]. The unknowns are the x and y components. The Doppler frequency is

$$f_d = \frac{2\overline{U_w}\cdot\overline{r}}{\lambda} \tag{6}$$

where

$$\bar{r}=\sin\theta\cos\phi\,\bar{x}+\sin\theta\sin\phi\,\bar{y}-\cos\theta\,\bar{z} \tag{7}$$

which stands for the antenna pointing vector.

## *Point solution*

To obtain the exact solution for the two unknowns, $U_{wx}$ and $U_{wy}$, from the two looks at each point, we write the Doppler velocity for two looks as

$$\begin{aligned} U_{d1}&=\bar{U}_w\cdot\bar{r}_1 \\ U_{d2}&=\bar{U}_w\cdot\bar{r}_2 \end{aligned} \tag{8}$$

where $r_1$ and $r_2$ are

$$\begin{aligned} \bar{r}_1&=\sin\theta\cos\phi_1\,\bar{x}+\sin\theta\sin\phi_1\,\bar{y}-\cos\theta\,\bar{z} \\ \bar{r}_2&=\sin\theta\cos\phi_2\,\bar{x}+\sin\theta\sin\phi_2\,\bar{y}-\cos\theta\,\bar{z} \end{aligned} \tag{9}$$

Solving (8), we obtain the solution in matrix form

$$\begin{pmatrix} U_{wx} \\ U_{wy} \end{pmatrix} = \begin{pmatrix} \sin\theta\cos\phi_1 & \sin\theta\sin\phi_1 \\ \sin\theta\cos\phi_2 & \sin\theta\sin\phi_2 \end{pmatrix} \begin{pmatrix} U_{d1}+U_{wz}\cos\theta \\ U_{d2}+U_{wz}\cos\theta \end{pmatrix} \tag{10}$$

The point solution gives the true wind velocity if the measurements have no errors. However, from the distribution of measured points (Fig. 3), we know that it is difficult to have two looks (one forward and the other backward) exactly at one point. We have to make pairs of measurements that may not be at the same locations, which introduces some geometrical errors.

The global wind models use cells of size 100km x 100km or larger. Thus, it is possible to use multiple points inside such a cell to derive the true wind velocity in that area. This is the cell solution or multiple-points solution.

## *Cell solution*

The cell solution groups the measured point distribution in a different way than the point solution. It divides the swath width into several bands according to the resolution requirements. The bands are cut into cells. Each cell is a square area with each side satisfying the resolution requirements. The number of looks in each cell depends on the distribution of the measured points. Fig. 4 depicts the bands, cells, and the number of points in each cell. The cells shown are square, with the 94-km dimension obtained by dividing the swath into 8 equal bands.

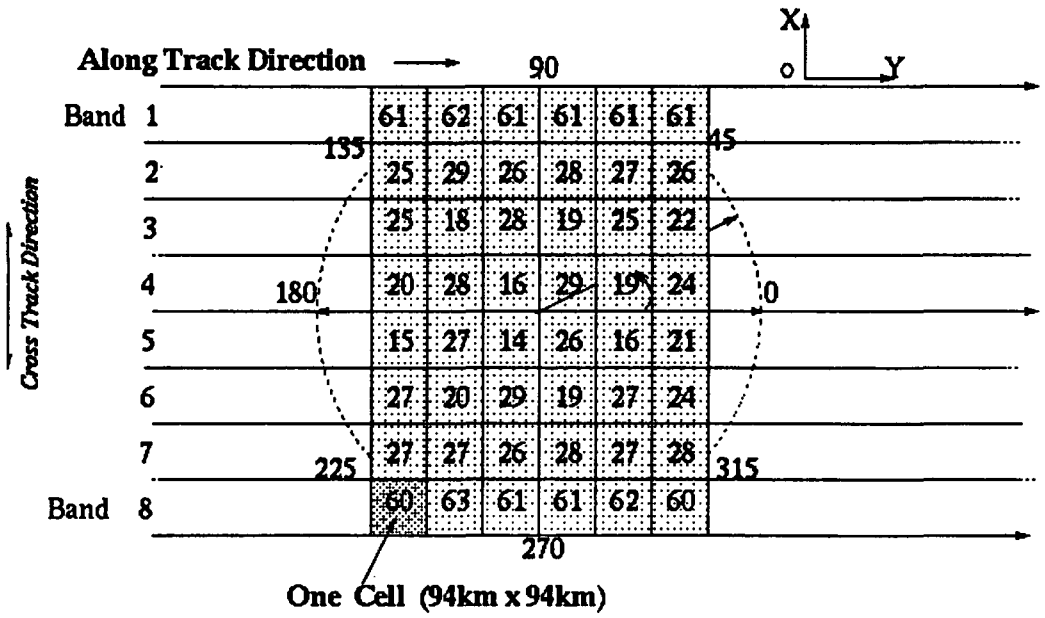


**Fig. 4. Measured location (bands and cells) and number of points in one cell for RAWS.**

In each cell, the estimated wind velocity can be calculated from the measured Doppler velocity for all the points inside that cell. Assuming the number of looks in the cell is N, then we write

$$U_{di}^{m} = U_{wx}\sin\theta\cos\phi_i + U_{wy}\sin\theta\sin\phi_i \qquad i=1,2,\ldots,N \qquad (11)$$

where $U^m_{di}$ is the measured Doppler velocity, and the z-direction component is known and is omitted. The square error between the measured and the true wind velocity is

$$\begin{aligned}\varepsilon &= \sum (U_{di} - U^m_{di})^2 \\ &= \sum [U_{di} - U_{wx}\sin\theta\cos\phi_i - U_{wy}\sin\theta\sin\phi_i]^2\end{aligned} \tag{12}$$

By taking the partial derivatives of $\varepsilon$ with respect to $U_{wx}$ and $U_{wy}$ and setting them to zero, we obtain

$$\begin{aligned}&\sum U_{di}\sin\theta\cos\phi_i - \sum \sin\theta\cos\phi_i [U_{wx}\sin\theta\cos\phi_i + U_{wy}\sin\theta\sin\phi_i] \\ &= \sum U_{di}\sin\theta\cos\phi_i - U_{wx}\sum \sin^2\theta\cos^2\phi_i + U_{wy}\sum \sin^2\theta\sin\phi_i\cos\phi_i \\ &\sum U_{di}\sin\theta\sin\phi_i - \sum \sin\theta\sin\phi_i [U_{wx}\sin\theta\cos\phi_i + U_{wy}\sin\theta\sin\phi_i] \\ &= \sum U_{di}\sin\theta\sin\phi_i - U_{wx}\sum \sin^2\theta\sin\phi_i\cos\phi_i + U_{wy}\sum \sin^2\theta\sin^2\phi_i\end{aligned} \tag{13}$$

Rearranging them to matrix format we get

$$\begin{pmatrix} \sum \sin^2\theta\cos^2\phi_i & \sum \sin^2\theta\sin\phi_i\cos\phi_i \\ \sum \sin^2\theta\sin\phi_i\cos\phi_i & \sum \sin^2\theta\sin^2\phi_i \end{pmatrix} \begin{pmatrix} U_{wx} \\ U_{wy} \end{pmatrix} = \begin{pmatrix} \sum U_{di}\sin\theta\cos\phi_i \\ \sum U_{di}\sin\theta\sin\phi_i \end{pmatrix}$$

(14)

The solution for this equation is

$$\begin{pmatrix} U_{wx} \\ U_{wy} \end{pmatrix} = \frac{1}{\sin\theta} \begin{pmatrix} \sum \cos^2\phi_i & \sum \sin\phi_i\cos\phi_i \\ \sum \sin\phi_i\cos\phi_i & \sum \sin^2\phi_i \end{pmatrix}^{-1} \begin{pmatrix} \sum U_{di}\cos\phi_i \\ \sum U_{di}\sin\phi_i \end{pmatrix} \tag{15}$$

Rewriting the inverse matrix in (15)

$$\begin{pmatrix} U_{wx} \\ U_{wy} \end{pmatrix} = \frac{1}{\sin\theta\,\Delta} \begin{pmatrix} \sum \sin^2\phi_i & -\sum \sin\phi_i \cos\phi_i \\ -\sum \sin\phi_i \cos\phi_i & \sum \cos^2\phi_i \end{pmatrix} \begin{pmatrix} \sum U_{di} \cos\phi_i \\ \sum U_{di} \sin\phi_i \end{pmatrix} \qquad (16)$$

where

$$\Delta = \sum \sin^2\phi_i \sum \cos^2\phi_i - \left(\sum \sin\phi_i \cos\phi_i\right)^2 \qquad (17)$$

# Error Analysis

Both the point solution and the cell solution give the exact wind velocity when there are no measurement errors. However, measurement errors are inevitable. The standard deviation of the average velocity for a covariance estimator is [8]

$$\Delta V_d = \lambda \left[ \left[ 32\pi^2 M \rho^2(T_s) T_s^2 \right]^{-1} \left[ \left[ (1-\rho^2(T_s)) \lambda \right] \frac{1}{[4\sigma_s T \pi^{1/2}]} + N^2/S^2 + 2(N/S) \right] \right]^{1/2} \qquad (18)$$

where M is the number of pulses for one look, $T_s$ is the spacing between the pulses of a pair, T is the pulse pair repetition time, $\sigma_s^2$ is the variance of the power spectral density of received echoes, and N/S is the inverse of signal-to-noise ratio. $\rho(T_s)$ is the correlation function [5]

$$\rho(mT_s) = \exp\left[ -8\left( \frac{\pi \sigma_s mT_s}{\lambda} \right)^2 \right] \qquad (19)$$

where m = 1 and $\lambda$ is the wavelength of the RF wave. To prevent the standard deviation $\Delta V_d$ from increasing exponentially and also to keep the samples correlated, $\sigma_s$ should satisfy

$$\sigma_s \leq \frac{\lambda}{4\pi T_s} \qquad (20)$$

Using carrier frequencies of 94 GHz, 24 GHz, and 35 GHz and the pulse period of Ts=207.8 μs, we calculated the standard deviations of the average Doppler velocity for a different numbers of pulses and SNR(signal to noise ratio). The results are shown in Tables 2 to 4.

**Table 2. The Standard Deviations of the Average Doppler Velocity at 94 GHz**

| Standard Deviation / Pulse Number / SNR | | Pulse Number Per Point (M) | | | |
|---|---|---|---|---|---|
| | | 128 | 256 | 512 | 1024 |
| SNR (dB) | 5 | 0.9749 | 0.6893 | 0.4874 | 0.3447 |
| | 10 | 0.6147 | 0.4346 | 0.3073 | 0.2173 |
| | 15 | 0.4670 | 0.3302 | 0.2335 | 0.1651 |
| | 20 | 0.4120 | 0.2913 | 0.2060 | 0.1457 |

**Table 3. The Standard Deviations of the Average Doppler Velocity at 24 GHz**

| Standard Deviation / Pulse Number / SNR | | Pulse Number Per Point (M) | | | |
|---|---|---|---|---|---|
| | | 128 | 256 | 512 | 1024 |
| SNR (dB) | 5 | 3.8182 | 2.6999 | 1.9091 | 1.3499 |
| | 10 | 2.4075 | 1.7024 | 1.2038 | 0.8512 |
| | 15 | 1.8292 | 1.2934 | 0.9146 | 0.6467 |
| | 20 | 1.6136 | 1.1410 | 0.8068 | 0.5705 |

Table 4. The Standard Deviations of the Average Doppler Velocity at 35 GHz

| Standard Deviation / Pulse Number / SNR | | Pulse Number Per Point (M) | | | |
|---|---|---|---|---|---|
| | | 128 | 256 | 512 | 1024 |
| SNR (dB) | 5 | 2.6182 | 1.8513 | 1.3091 | 0.9257 |
| | 10 | 1.6509 | 1.1673 | 0.8254 | 0.5837 |
| | 15 | 1.2534 | 0.8869 | 0.8254 | 0.4435 |
| | 20 | 1.1065 | 0.7824 | 0.5532 | 0.3912 |

A combination of increases in both the number of pulses and SNR will lower the standard deviations of the average Doppler velocity and thus help to provide a better estimate from the measurements. Note that the standard deviations decrease as we use higher RF frequencies.

As well as the measurement errors, the geometrical distribution of the points also contributes to the wind errors. Using the point-solution formula (10), we evaluate the dependence of wind errors on the location of the measured points. Fig. 5a and b show the wind errors at different azimuth angles, using 94 GHz as an example. A Monte Carlo approach (2000 trials) was used for the point-solution formula. The results in Fig. 6 show the probability of errors at different azimuth angles. For this example, a fixed error of 0.2 m/s is assumed for the radial velocity in the backward direction. The parameter for the curves is the error in forward radial velocities. It can be seen that larger errors occur near the edge area ( $\Phi \approx 90°$) and the center area ($\Phi \approx 0°$). The points near the edge and the center area must be discarded to meet the accuracy requirements. Hence, the uesful swath width is less than the diameter of the scan.

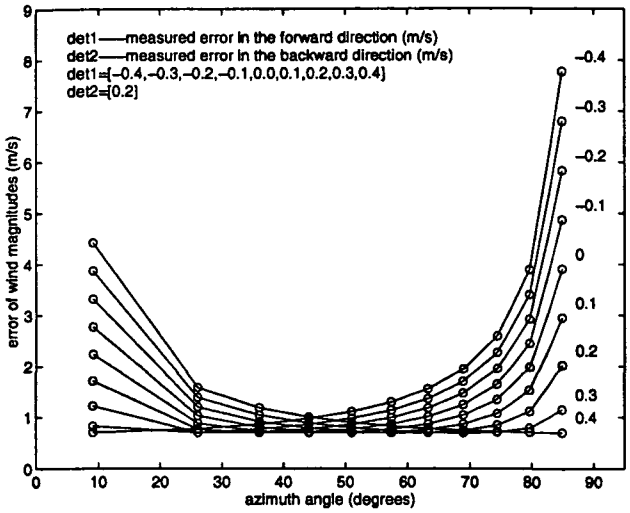


Fig. 5a. Wind magnitude errors.

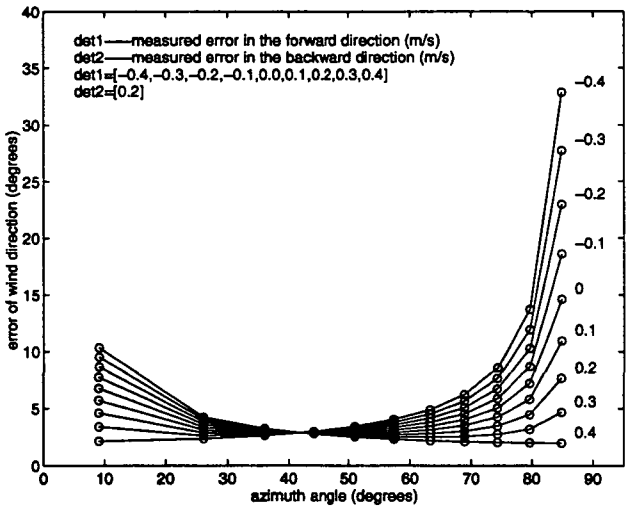


Fig. 5b. Wind direction errors.

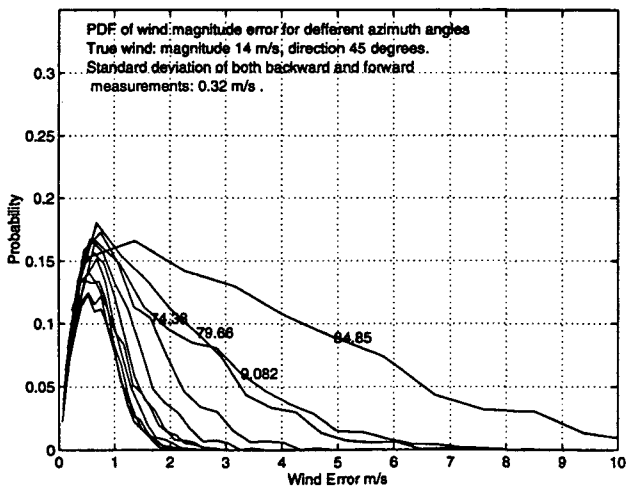


(a) PDF of the wind magnitude errors.

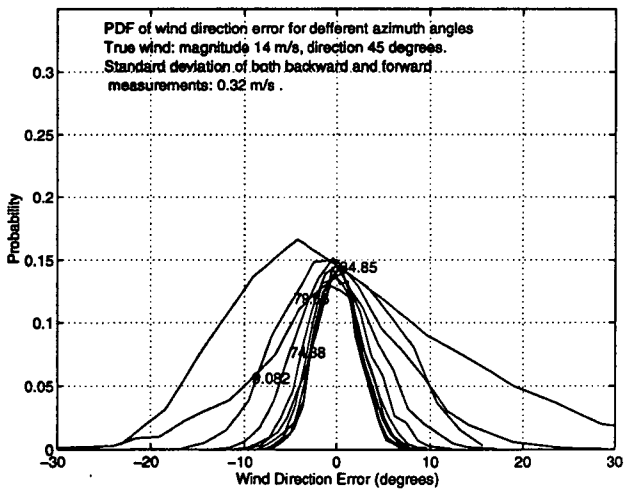


(b) PDF of the wind direction errors.

Fig. 6. Probability distribution of the wind errors (the numbers in the figures indicate the azimuth angles).

Even though the point solution gives an estimation of wind velocity at a single point, global wind modeling needs only one wind datum in a target area. The cell solution can be used to meet the requirements. Using (16) and (18), along with the measurement errors (assuming Gaussian), we develop an algorithm to simulate the errors in the measured winds. The results are presented in Figs. 7a and b to 9a and b. The conditions for each run of simulation are stated in brackets following the title of each figure.

Figs. 7a and b to 9a and b show the probability distribution of the magnitude and direction errors of a given wind velocity in different bands and cells (see Fig. 4). For the 94-GHz case, the simulated true wind magnitude errors rarely exceed 2 m/s and the true wind direction errors do not exceed ±15° with 90% probability. The 24-GHz case exhibits larger errors in both magnitude and direction than that at 94 GHz. The direction errors go beyond ±20° in bands #4 and #5 with 50% probability. The magnitude errors go beyond ±2 m/s in bands #1 and #8 with less than 5% probability; beyond 2m/s in bands #4 and #5 with 10% probability. With 35 GHz, the direction errors go beyond ±20° in bands #4 and #5 with 10% probability, and the magnitude errors are within ±2 m/s in every band with 90% probability. The simulated results indicate that maximum errors are concentrated in the center area (bands #4 and #5).

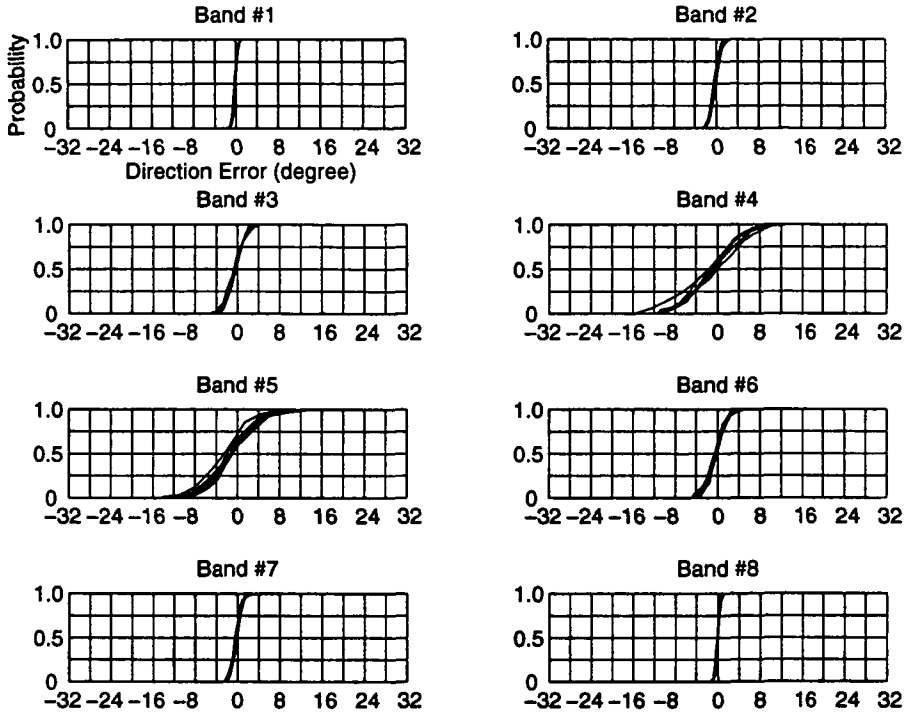


Fig. 7a. Probability distribution of the direction errors (true wind: 14m/s at 0°; 256 pulses/point; cell size: 94km x 94km; SNR = 10dB; Freq = 94GHz).

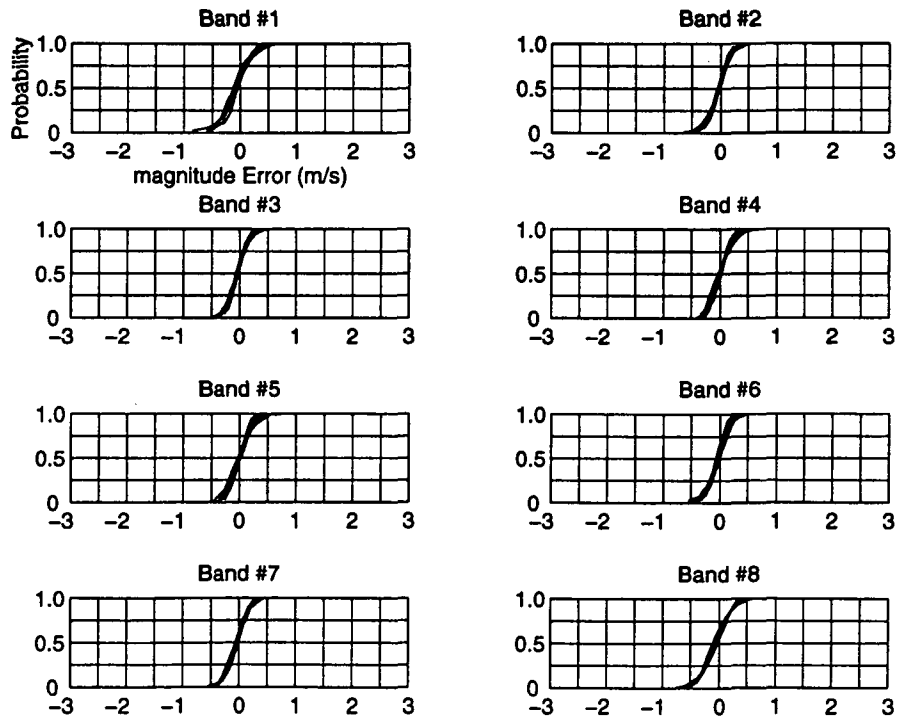


Fig. 7b. Probability distribution of the magnitud errors (true wind: 14m/s at 0°; 256 pulses/point; cell size: 94km x 94km; SNR = 10dB; Freq = 94GHz).

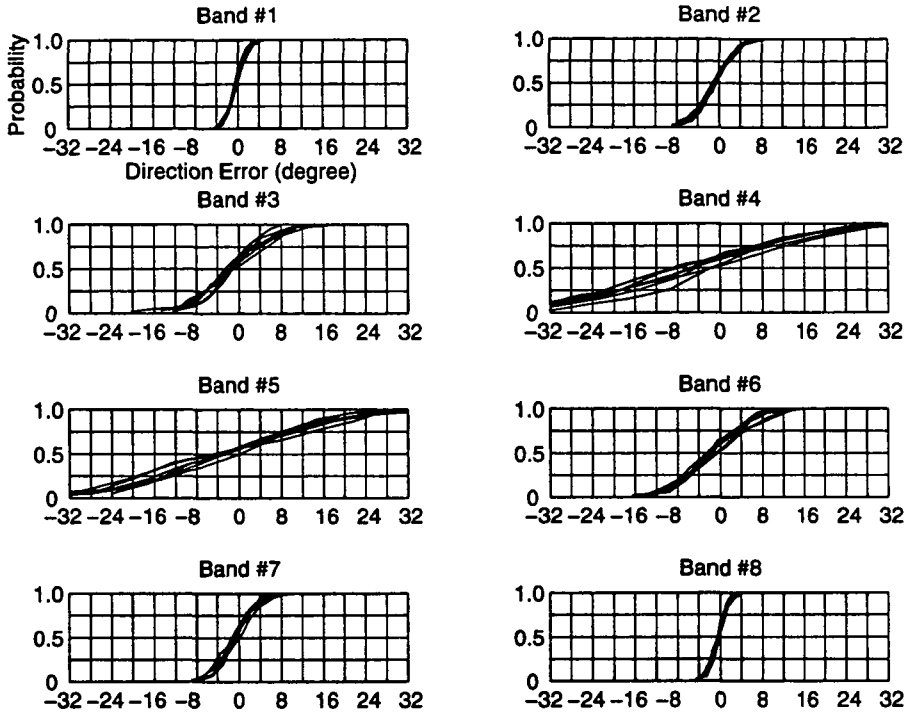


Fig. 8a. Probability distribution of the direction errors (true wind: 14m/s at 0°; 256 pulses/point; cell size: 94km x 94km; SNR = 10dB; Freq = 24GHz).

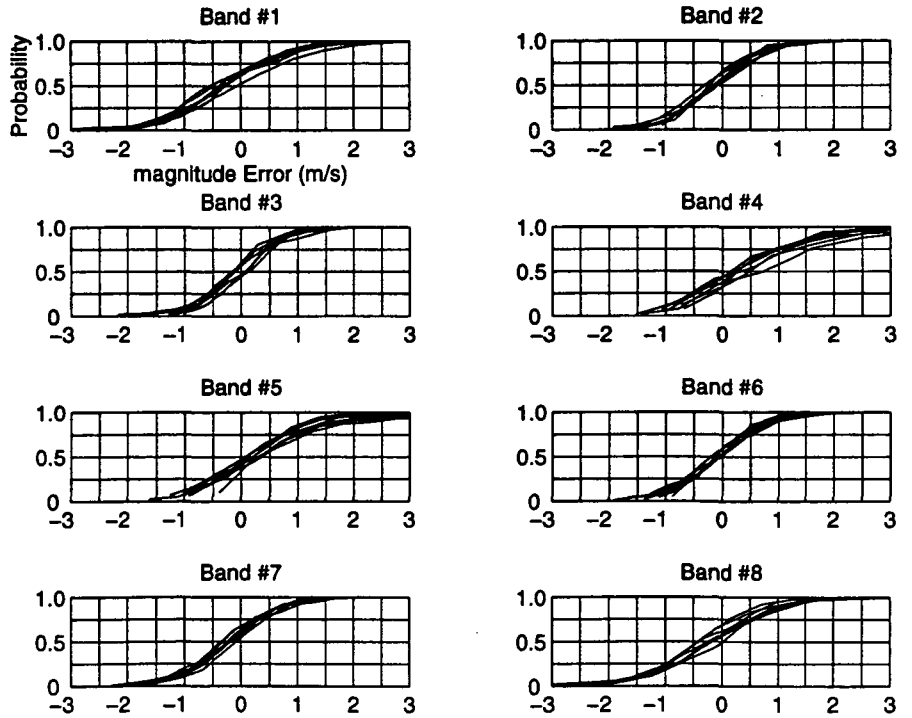


Fig. 8b. Probability distribution of the magnitude errors (true wind: 14m/s at 0°; 256 pulses/point; cell size: 94km x 94km; SNR = 10dB; Freq = 24GHz).

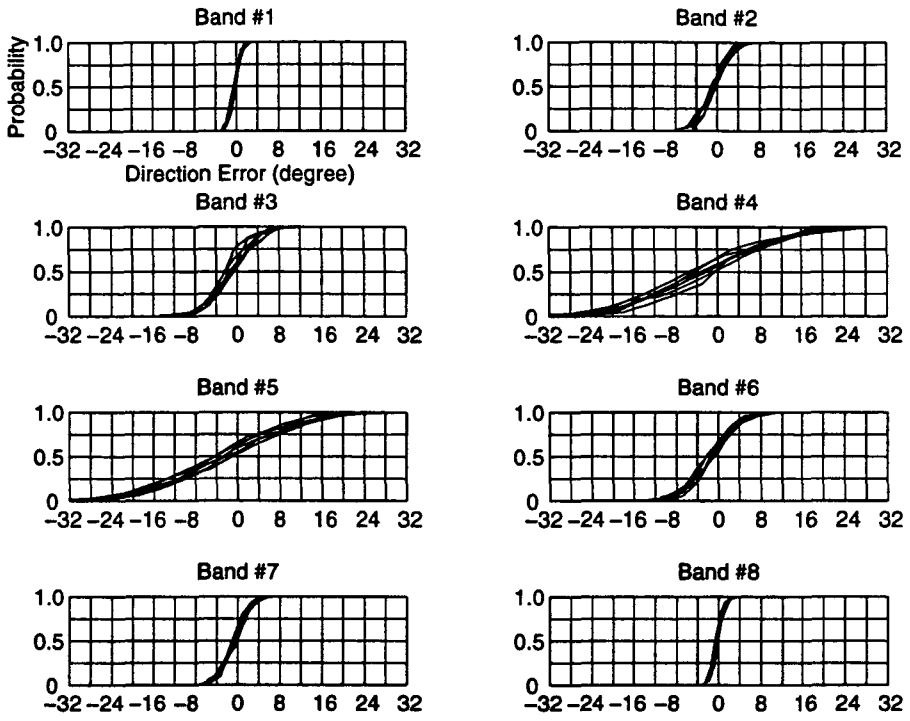


Fig. 9a. Probability distribution of the direction errors (true wind: 14m/s at 0°; 256 pulses/point; cell size: 94km x 94km; SNR = 10dB; Freq = 35GHz).

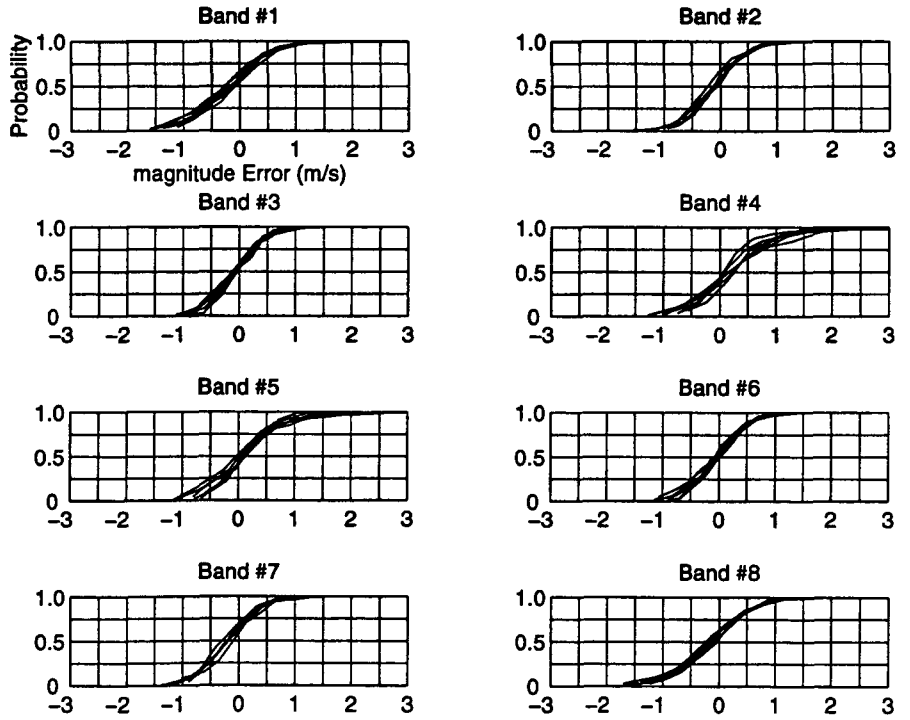


Fig. 9b. Probability distribution of the magnitude errors (true wind: 14m/s at 0°; 256 pulses/point; cell size: 94km x 94km; SNR = 10dB; Freq = 35GHz).

The errors of the measured wind also depend on the magnitude and direction of the true wind. Figs. 10a and b to 12a and b show the RMS (Root Mean Square) errors for four different wind speeds, namely 5 m/s, 8 m/s, 10 m/s and 14 m/s. The change in true wind magnitude does not affect the magnitude errors significantly, but it does have strong influence on the direction errors. At 94 GHz, the RMS errors for the wind direction are within 20° and the magnitude errors are well below 1 m/s at all the bands. At 24 GHz, the direction RMS errors exceed 20° in bands #4 and #5 for true wind speeds of 5 m/s, 8 m/s and 10 m/s. For bands #4 and #5, we also see the RMS errors for the wind magnitudes go beyond 2 m/s, except in the 14-m/s case. With 35 GHz, the RMS errors for the derived wind direction exceed 20° at bands #4 and #5 when the true wind speed is 8 m/s or below. The magnitude RMS errors are below 2 m/s. All the figures display the trend of decrease in direction errors as the measured wind speeds increase. Except for the center bands (#4 and #5) for the 24-GHz and 35-GHz cases, the overall errors at other bands fall below 20° and 2 m/s, which is the specification for RAWS.

The number of pulses averaged for each point also influences the errors. Figs. 13a and b to 15a and b illustrate the simulation results using four different numbers of pulses, 128, 256, 512 and 1024. Averaging more pulses for one point would decrease the errors but would also decrease the number of measured points within one cell. Too few pulses per point would cause a larger standard deviation (see Tables 2 to 4). For all the 94-GHz, 24-GHz and 35-GHz cases, we found that the tradeoff between averaging more pulses and getting more measured points results in comparable errors except when using 1024 pulses per point. With 1024 pulses per point, reducing the standard deviation can no longer compensate the error due to fewer measured points in a cell. For the time being, we find that 256 pulses per point is suitable.

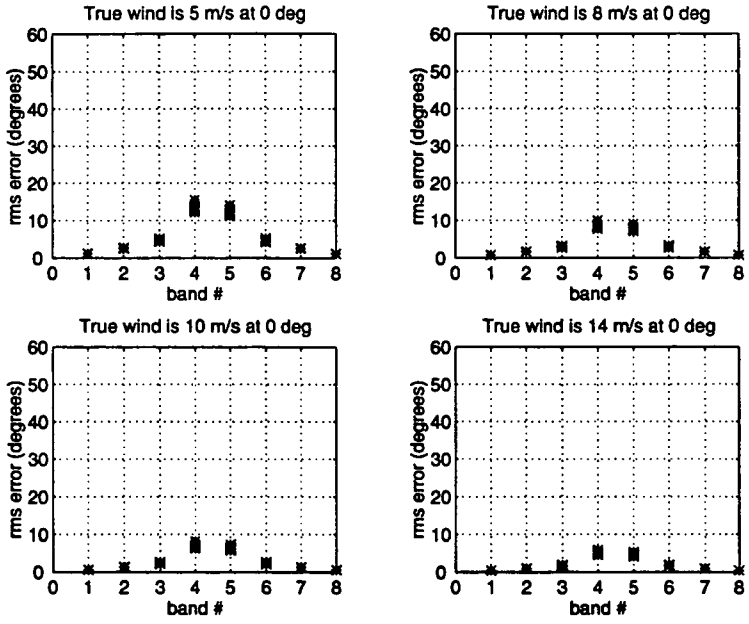


Fig. 10a. RMS erorrs of wind direction for different wind magnitudes (256 pulses/point; cell size: 94kmx94km; SNR = 10dB; Freq = 94GHz).

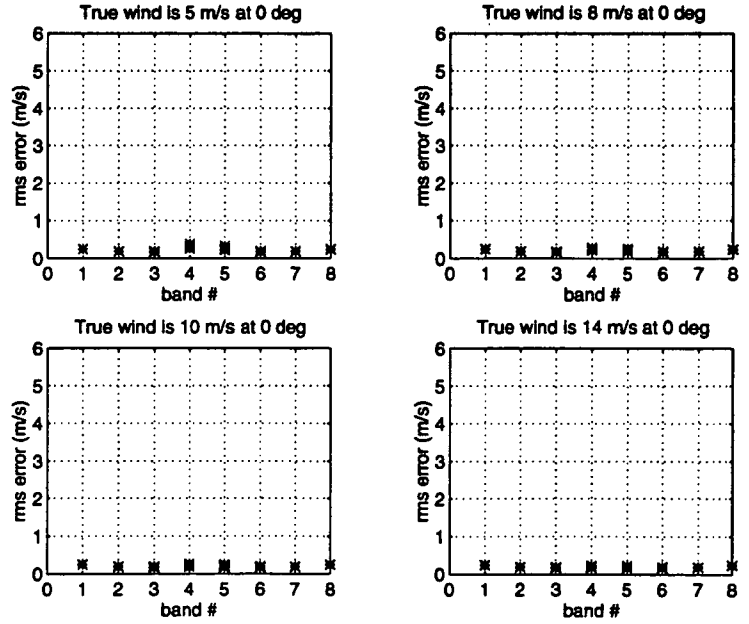


Fig. 10b. RMS erorrs of wind magnitude for different wind magnitudes (256 pulses/point; cell size: 94kmx94km; SNR = 10dB; Freq = 94GHz).

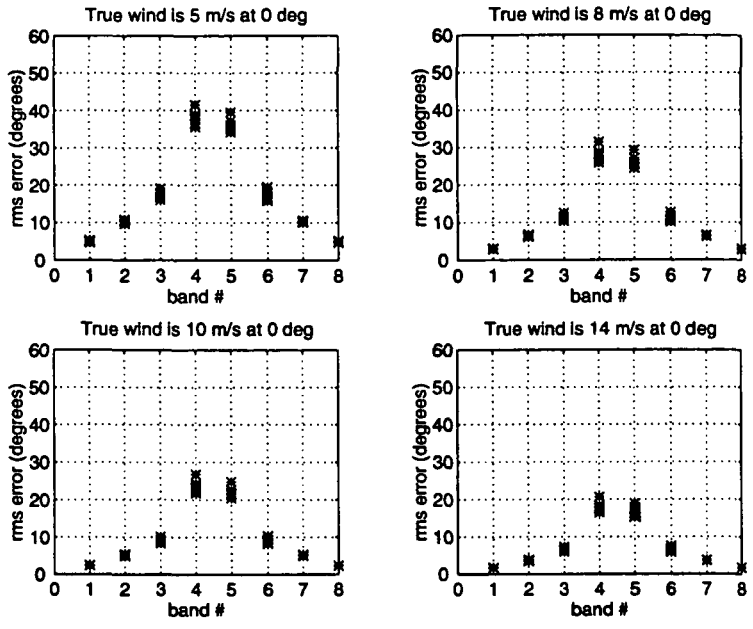


Fig. 11a. RMS erorrs of wind direction for different wind magnitudes (256 pulses/point; cell size: 94kmx94km; SNR = 10dB; Freq = 24GHz).

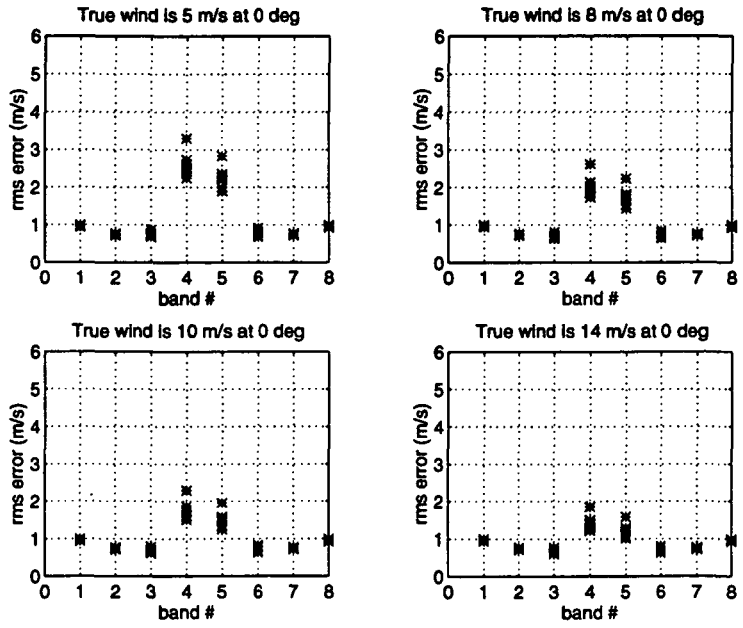


Fig. 11b. RMS erorrs of wind magnitude for different wind magnitudes (256 pulses/point; cell size: 94kmx94km; SNR = 10dB; Freq = 24GHz).

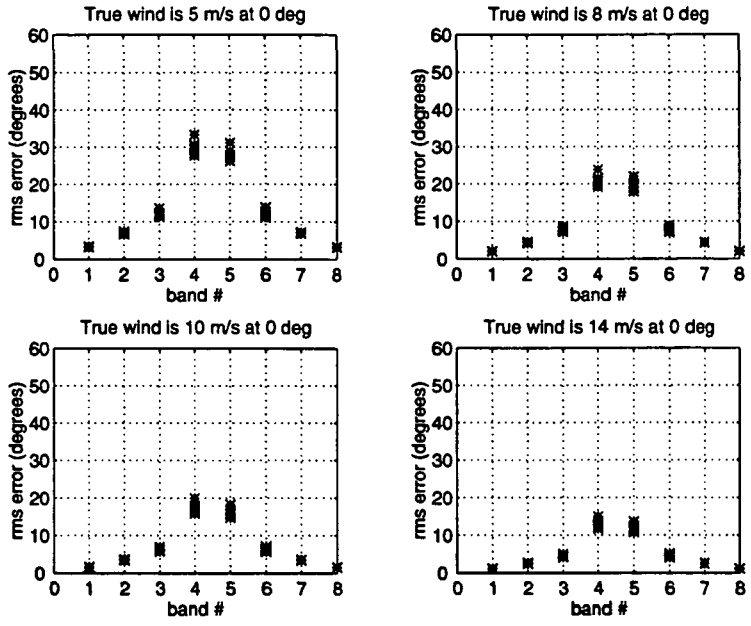


Fig. 12a. RMS erorrs of wind direction for different wind magnitudes (256 pulses/point; cell size: 94kmx94km; SNR = 10dB; Freq = 35GHz).

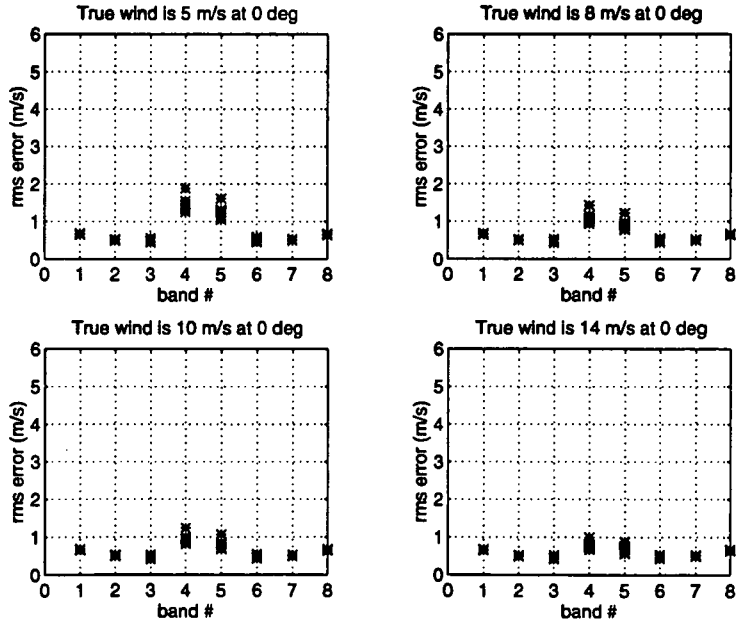


Fig. 12b. RMS erorrs of wind magnitude for different wind magnitudes (256 pulses/poi'nt; cell size: 94kmx94km; SNR = 10dB; Freq = 35GHz).

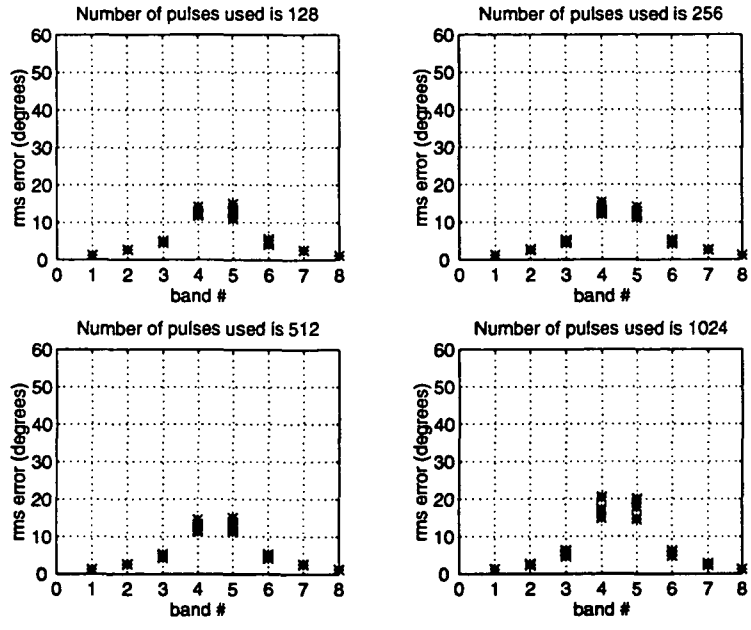


Fig. 13a. RMS errors of wind direction for different number of pulses per point (true wind: 5m/s at 0°; cell size: 94km x 94km; SNR = 10dB; Freq = 94GHz).

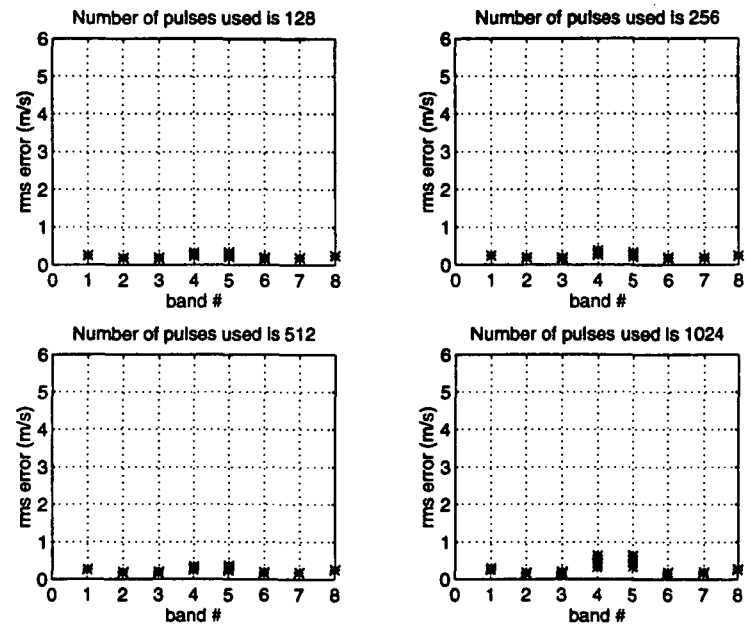


Fig. 13b. RMS errors of wind magnitude for different number of pulses per point (true wind: 5m/s at 0°; cell size: 94km x 94km; SNR = 10dB; Freq = 94GHz).

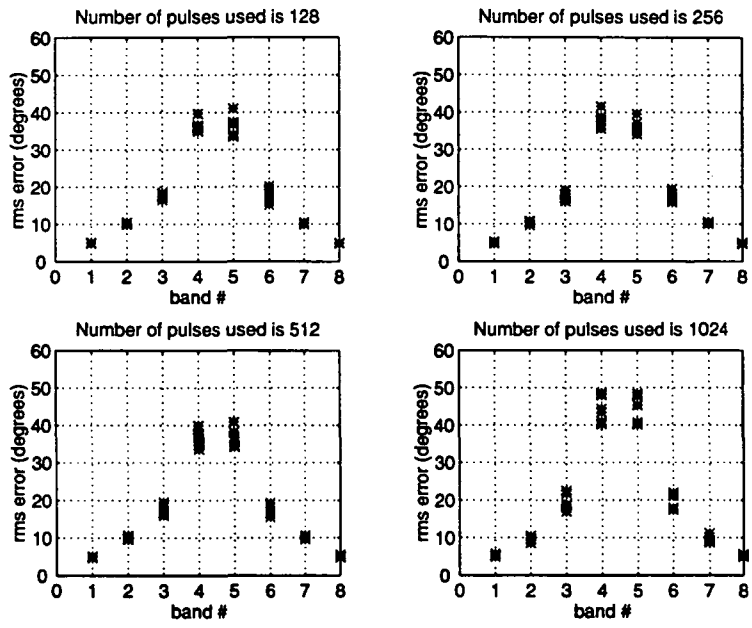


Fig. 14a. RMS errors of wind direction for different number of pulses per point (true wind: 5m/s at 0°; cell size: 94km x 94km; SNR = 10dB; Freq = 24GHz).

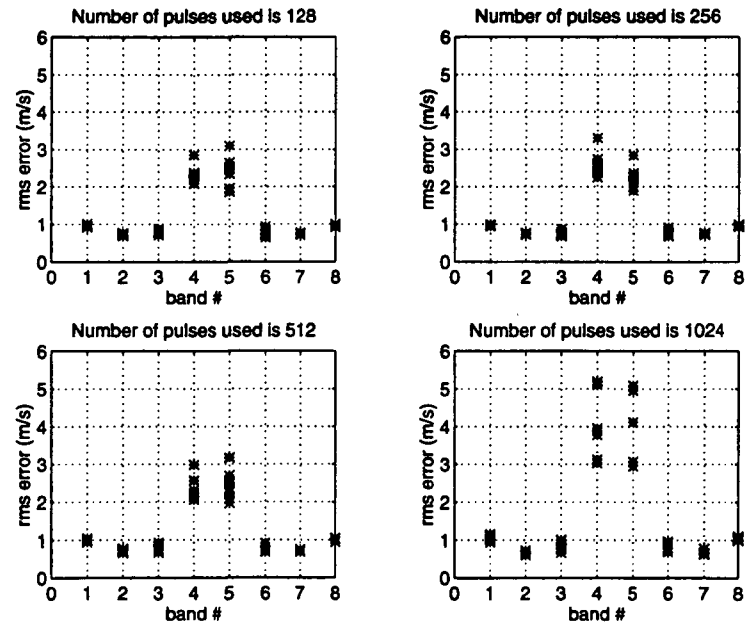


Fig. 14b. RMS errors of wind magnitude for different number of pulses per point (true wind: 5m/s at 0°; cell size: 94km x 94km; SNR = 10dB; Freq = 24GHz).

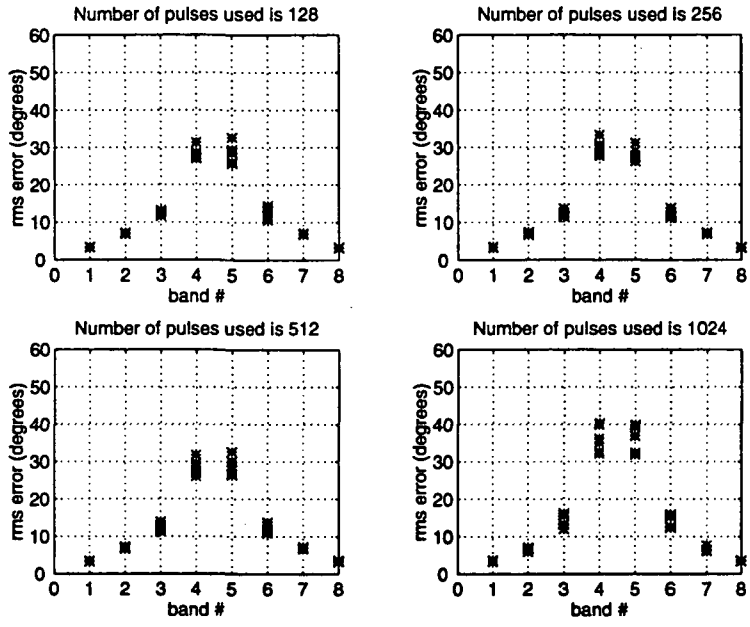


Fig. 15a. RMS errors of wind direction for different number of pulses per point (true wind: 5m/s at 0°; cell size: 94km x 94km; SNR = 10dB; Freq = 35GHz).

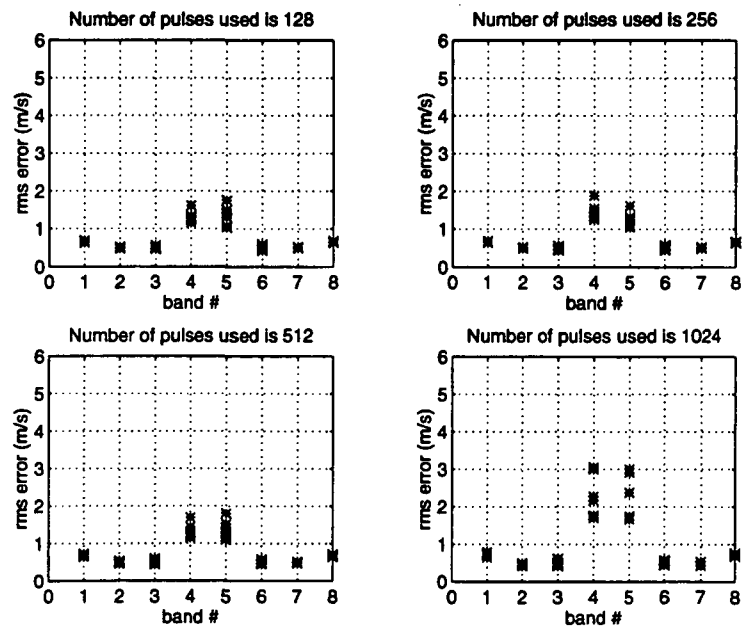


Fig. 15b. RMS errors of wind magnitude for different number of pulses per point (true wind: 5m/s at 0°; cell size: 94km x 94km; SNR = 10dB; Freq = 35GHz).

The errors also depend on the cell sizes. Larger cells have more points, allowing more averaging to make the solution more accurate. Fig. 16a, b and c compares the simulation results for cells with different sizes at 94 GHz, 24 GHz and 35 GHz, respectively. For this simulation, we chose the cell sizes to be 94 km x 66 km and 94 km x 132 km. We chose 66 km so that the cells along each band will have the same number of measured points (for spacecraft velocity of 6.6 km/s and scan periods of 10 s). With an along-track distance of 132 km, there will be twice as many points as in the 66-km size. The results show that larger cells give lower RMS errors in both the wind direction and magnitude.

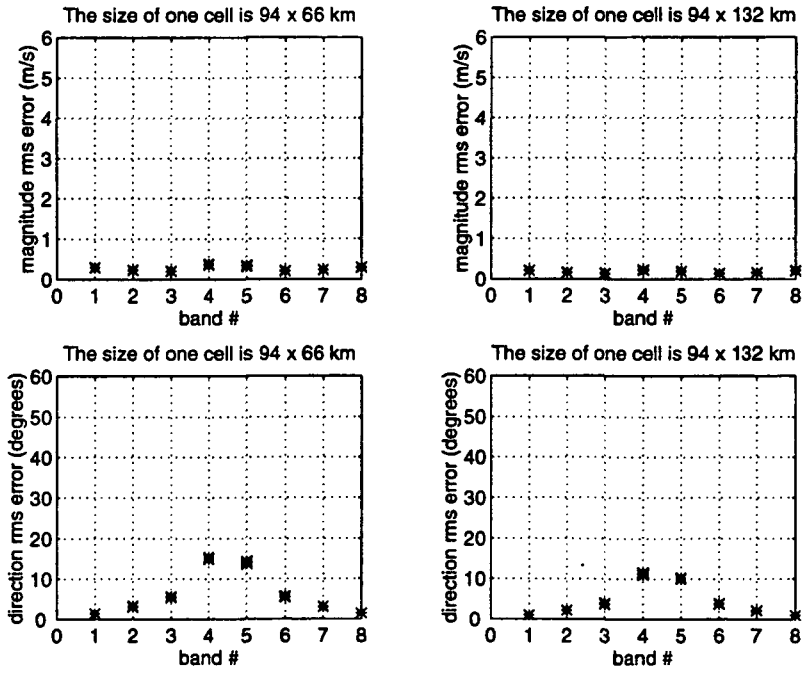


Fig. 16a. RMS errors of wind for different cell sizes (true wind: 5m/s at 0°; 256 pulses/point; SNR = 10dB; Freq = 94GHz).

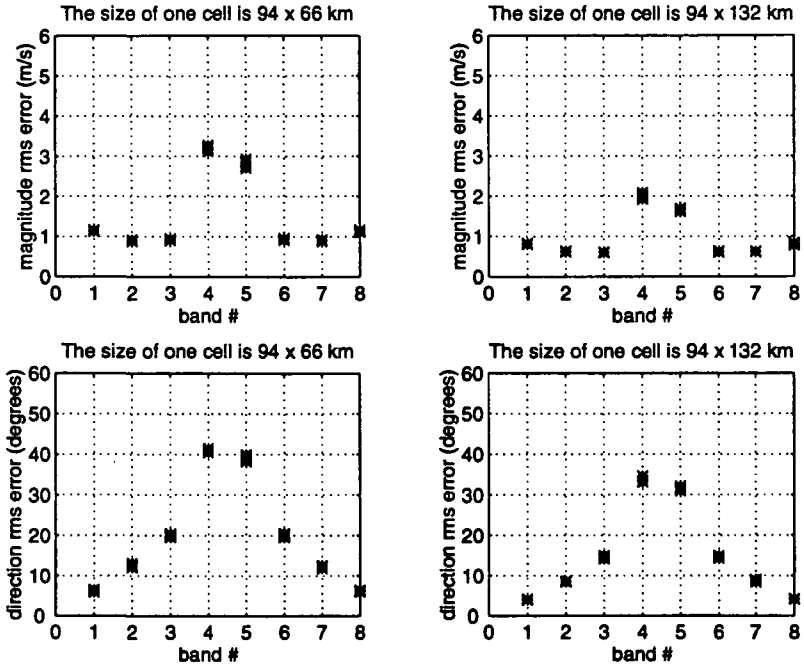


Fig. 16b. RMS errors of wind for different cell sizes (true wind: 5m/s at 0°; 256 pulses/point; SNR = 10dB; Freq = 24GHz).

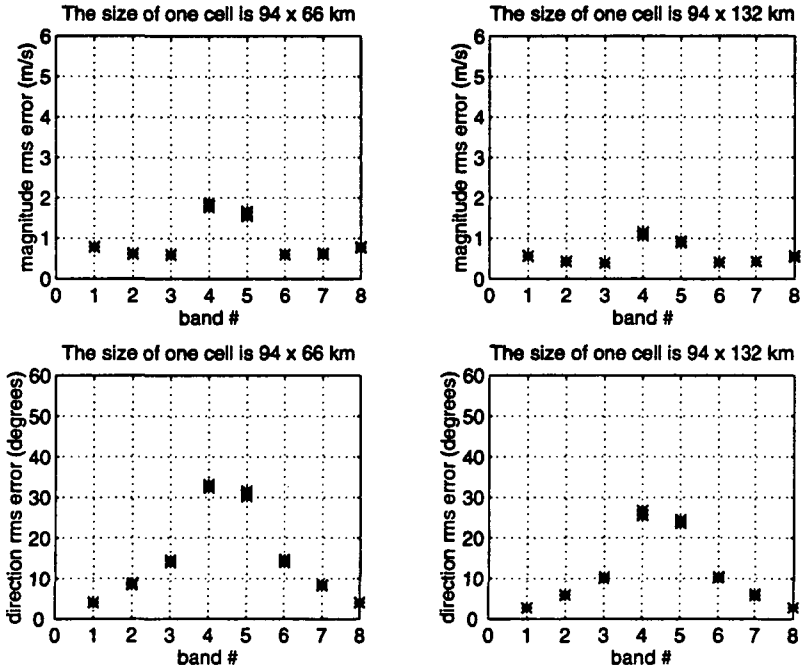


Fig. 16c. RMS errors of wind for different cell sizes (true wind: 5m/s at 0°; 256 pulses/point; SNR = 10dB; Freq = 35GHz).

The SNR is another important factor that influences the RAWS accuracy. Increasing the SNR would decrease the standard deviation (see Tables 2 to 4) and thus reduce the measurement errors, but this requires increasing the transmitting power. For this sensitivity study, we chose SNR = 10 dB as a suitable compromise.

# Optimize the cell size

Earlier simulation results show high RMS errors at the center bands for the 24-GHz and 35-GHz cases for low wind speeds (5 m/s in our simulations). We also showed that the RMS errors, especially the direction errors, can be reduced by increasing the cell size, allowing more measurement points to be averaged. The simulation results indicate a smaller cell size in bands #1,#2 and #7,#8 is possible, which allows retaining the RMS errors below the specifications. These observations suggest using a larger cell size in the center bands and a smaller cell size in the outer bands.

Further simulations were performed to evaluate the possibility of using a cell size of 66 km x 66 km for the outer bands ( #1,#2,#7,#8) and a cell size of 132 km x 132 km for the center bands (#3,#4.#5,#6). To maintain an 8-band resolution within the swath, we allow the cells on bands #3 and #4 to overlap one another partially. We do the same for the cells on bands #5 and #6. Noisy wind speeds of 5 m/s and 14 m/s, each with directions at 0°, 45° and 90°, were chosen as the input winds for the simulations.

Figs. 17 to 22 illustrate the following observations:

(a) At 5 m/s, the direction errors at the center bands are slightly above 20° for the 24-GHz cases and below 20° for the 35-GHz cases. The magnitude errors are less than 2 m/s in all cases except one, the 24-GHz case with wind direction at 90°.

(b) At 14 m/s, both the direction and magnitude errors are below 20° and 2 m/s in all cases except one, the 24-GHz case with wind direction at 90°, where the magnitude error is slightly above 2 m/s.

The results demonstrate the feasibility of using these multiple cell sizes to achieve a better wind vector estimation.

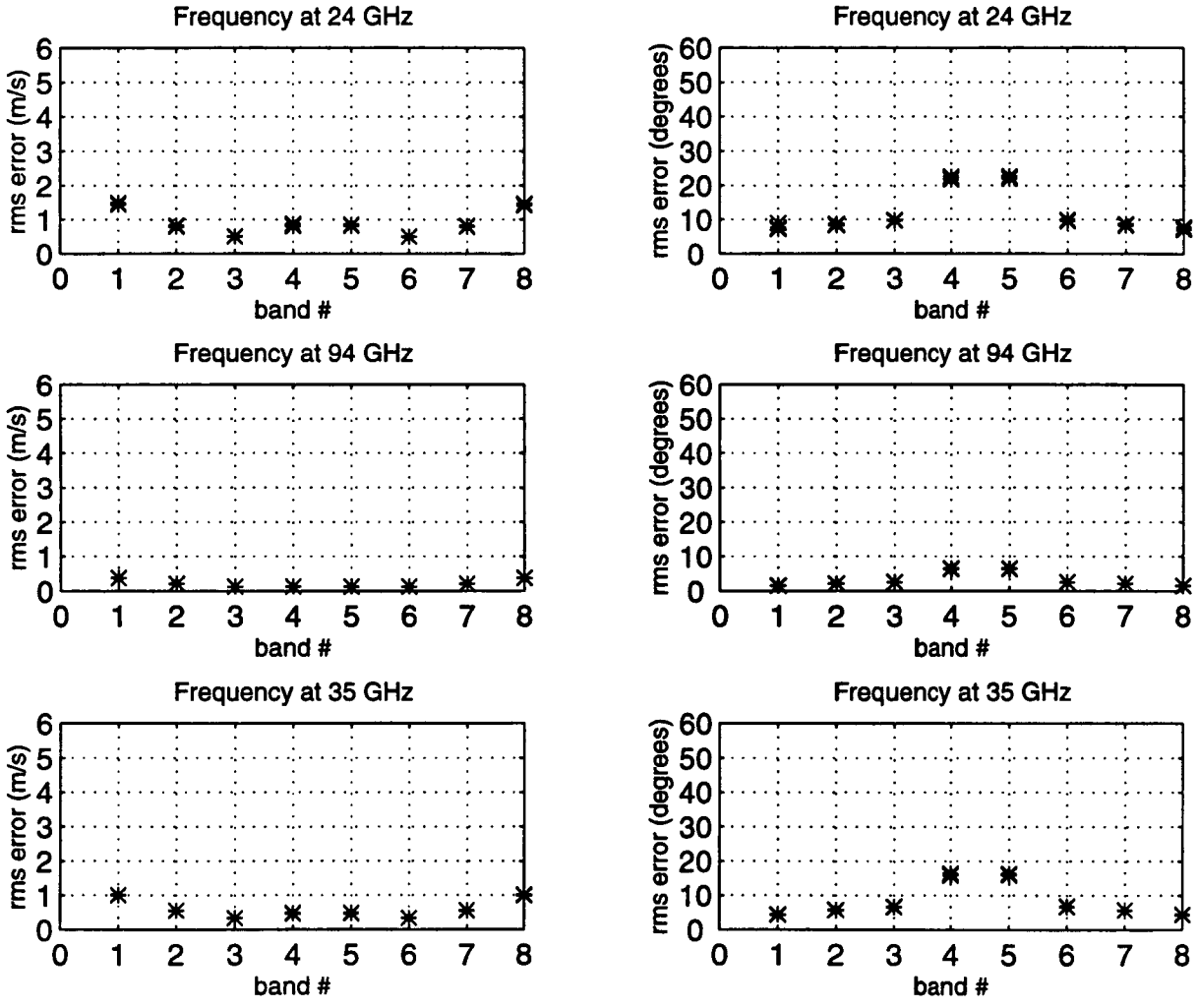


Fig. 17. RMS errors of wind vectors using cell size of 66km x 66km for bands #1,2,7,8 and 132km x 132km for bands #3,4,5,6 (true wind: 5 m/s at 0°; 256 pulses/point; SNR = 10dB).

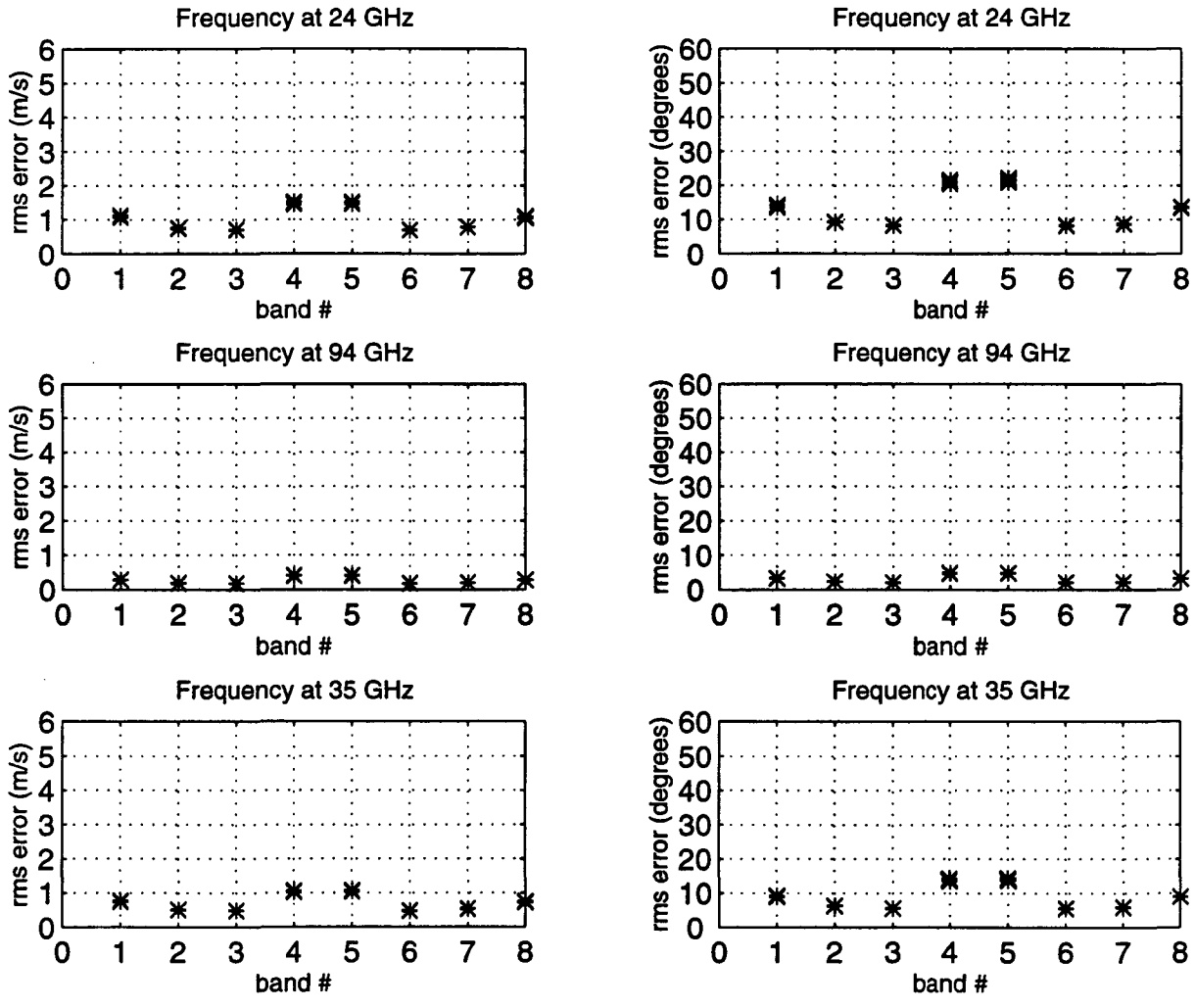


Fig. 18. RMS errors of wind vectors using cell size of 66km x 66km for bands #1,2,7,8 and 132km x 132km for bands #3,4,5,6 (true wind: 5 m/s at 45°; 256 pulses/point; SNR = 10dB).

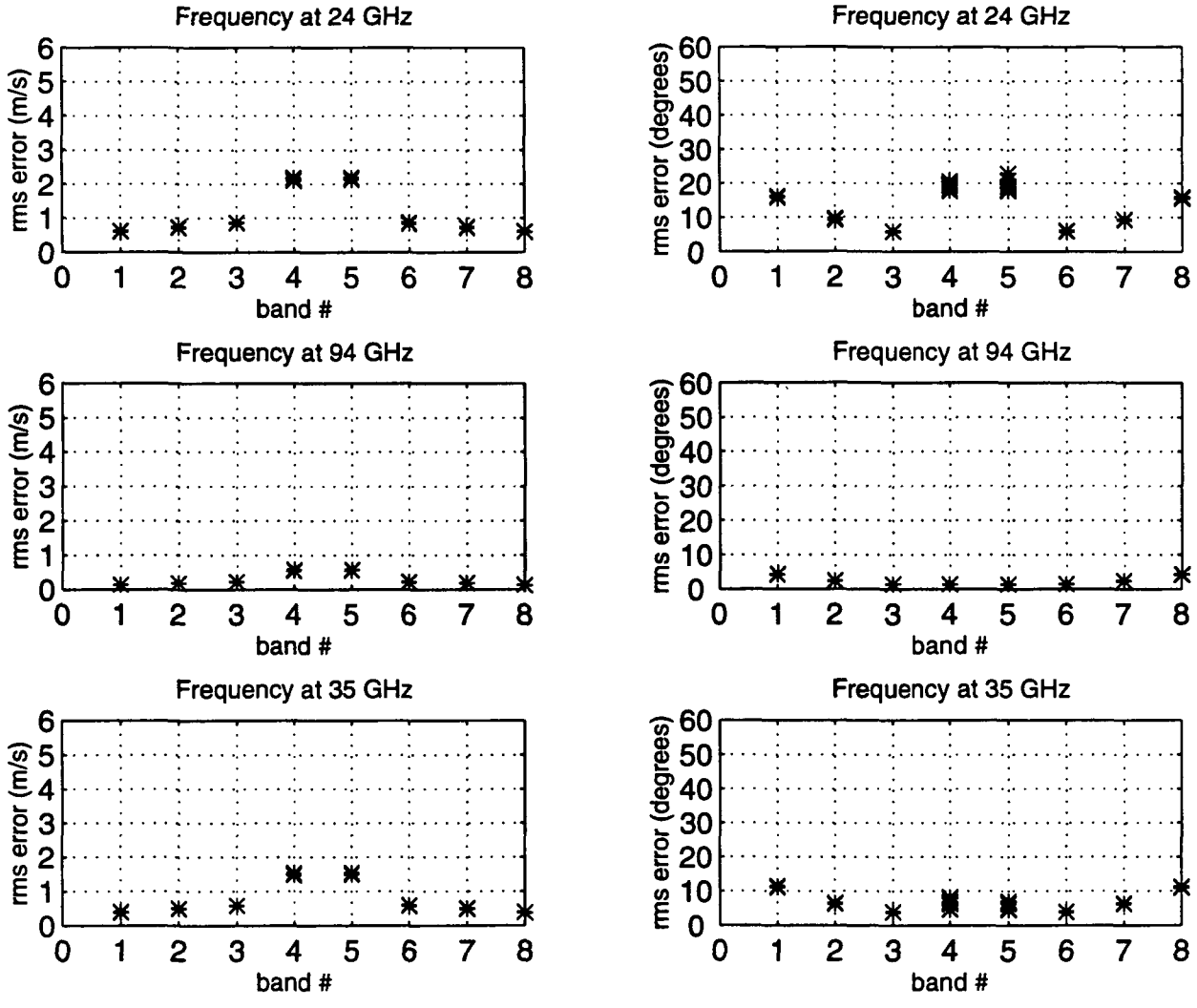


Fig. 19. RMS errors of wind vectors using cell size of 66km x 66km for bands #1,2,7,8 and 132km x 132km for bands #3,4,5,6 (true wind: 5 m/s at 90°; 256 pulses/point; SNR = 10dB).

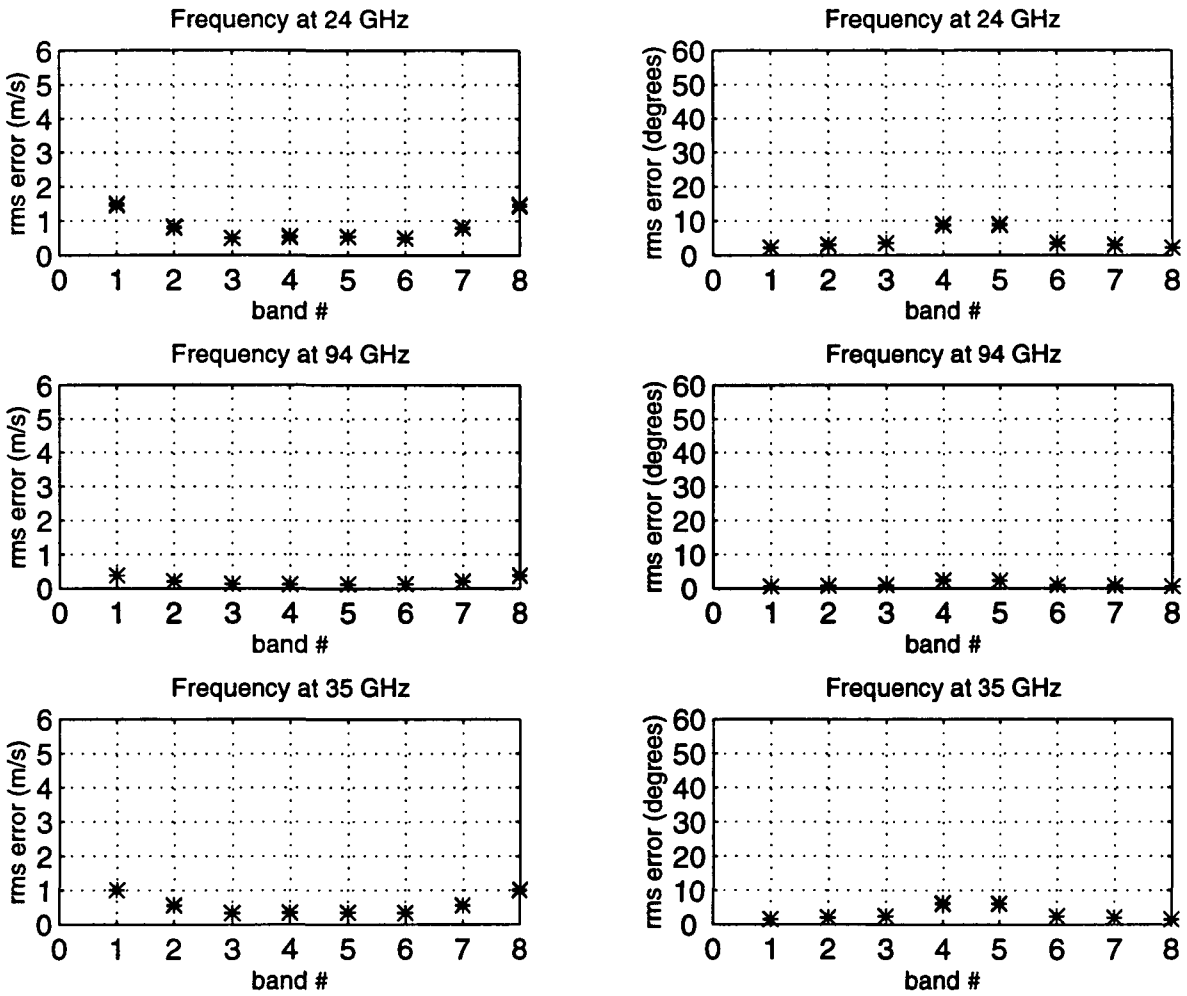


Fig. 20. RMS errors of wind vectors using cell size of 66km x 66km for bands #1,2,7,8 and 132km x 132km for bands #3,4,5,6 (true wind: 14 m/s at 0°; 256 pulses/point; SNR = 10dB).

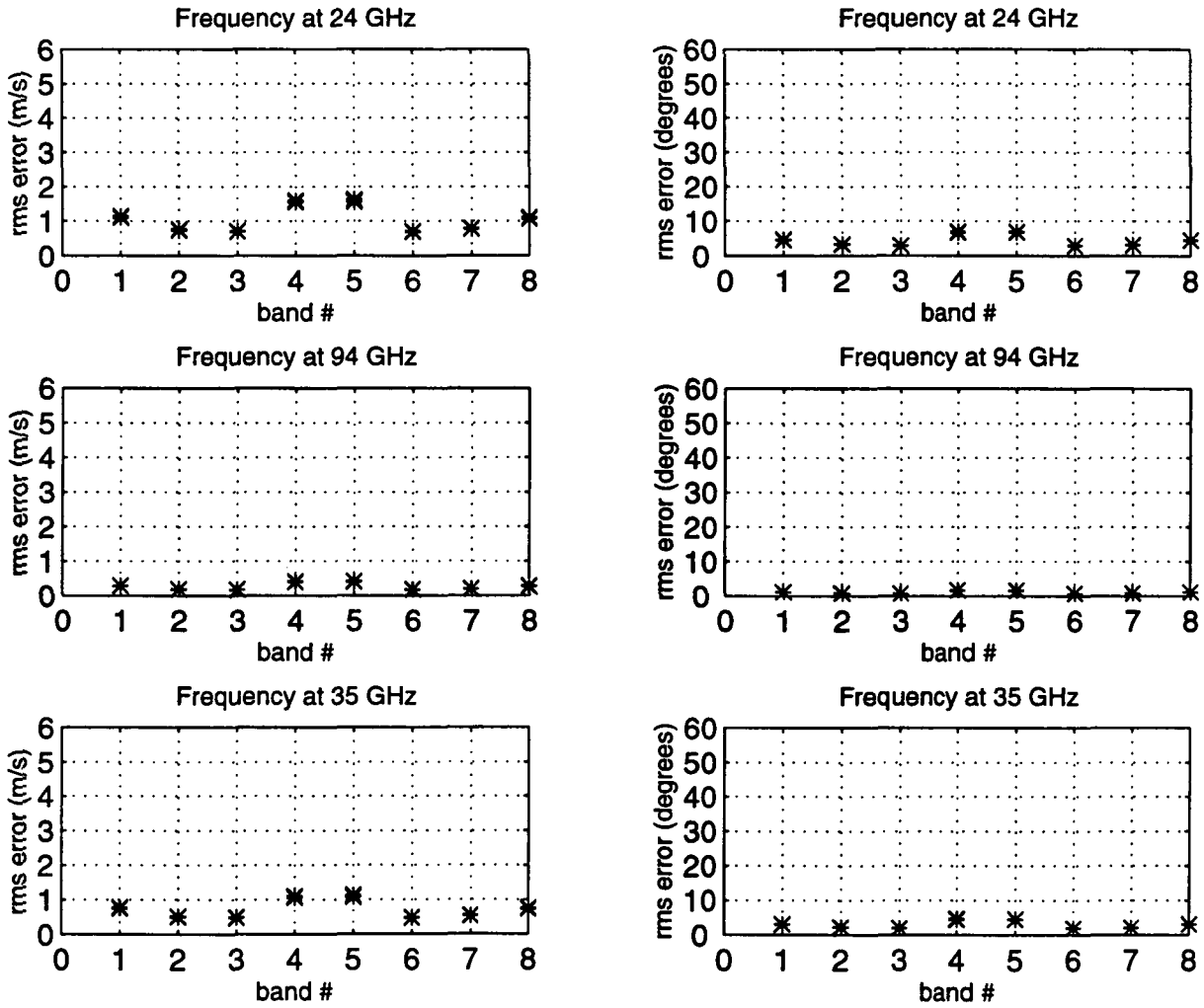


Fig. 21. RMS errors of wind vectors using cell size of 66km x 66km for bands #1,2,7,8 and 132km x 132km for bands #3,4,5,6 (true wind: 14 m/s at 45°; 256 pulses/point; SNR = 10dB ).

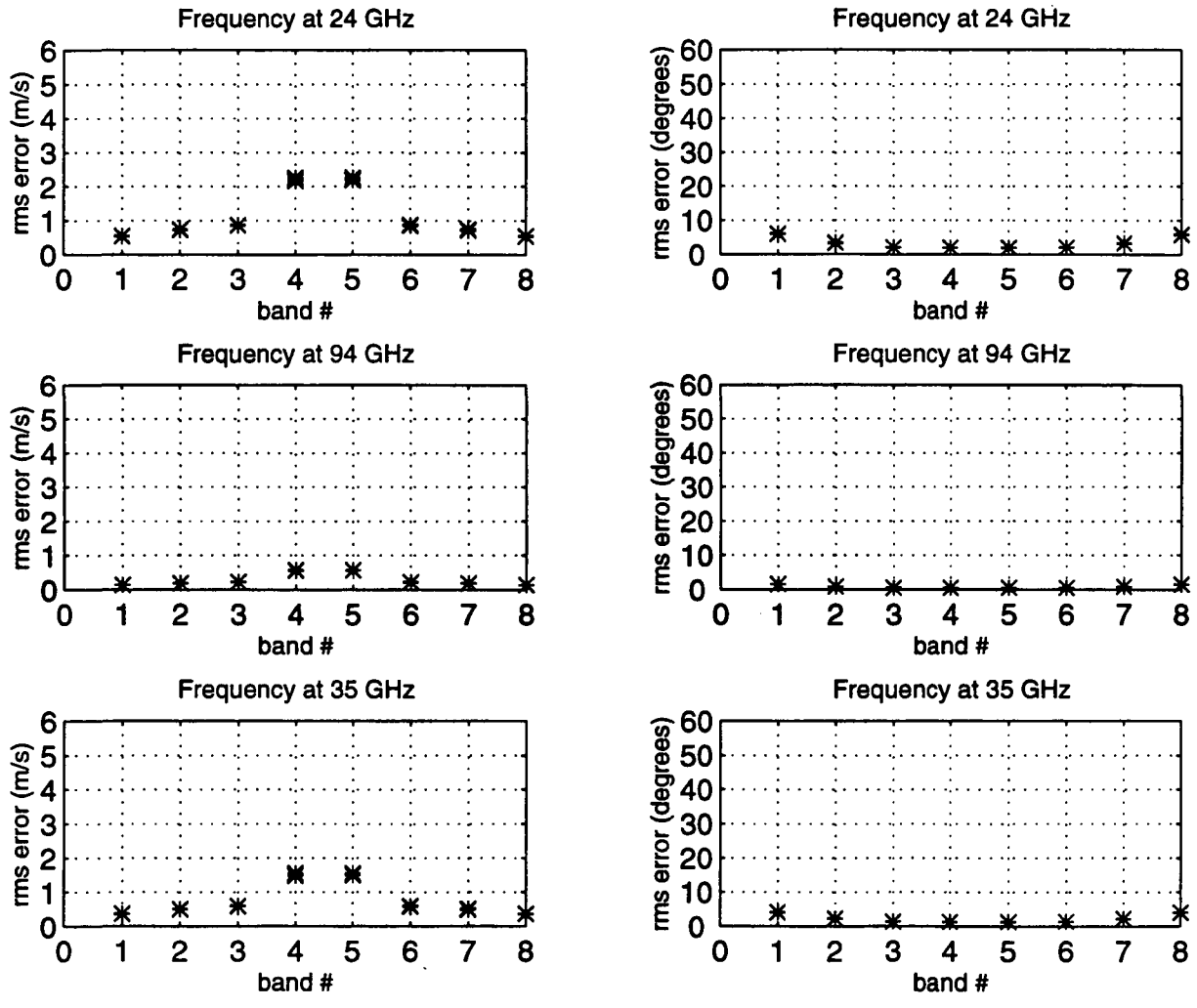


Fig. 22. RMS errors of wind vectors using cell size of 66km x 66km for bands #1,2,7,8 and 132km x 132km for bands #3,4,5,6 (true wind: 14 m/s at 90°; 256 pulses/point; SNR = 10dB ).

# Discussion and Conclusions

The simulation results shown here indicate that RAWS can provide measurements of winds aloft with adequate accuracy for use in global atmospheric models. However, the accuracy was achieved by combining multiple measurements from relatively large areas (66-km x 66-km cells and 132-km x 132-km cells). Clearly, many such cells will not be covered entirely by hydrometeors, so the numbers of measurements available for averaging will be less than used here. If we tried to use RAWS alone, the errors incurred when cells are only partially cloud covered would exceed the values in our simulations.

Since the purpose of RAWS is to provide wind measurements in cloud-covered areas, and since it would normally be used with a laser wind sensor, the Doppler measurements from the radar and laser systems should be combined for partially covered cells. We did not simulate this situation, but one would expect similar, yet different, results. The laser scan pattern would be similar to that of the radar, but its shot rate would differ, and the errors of individual measurements would differ from those of the radar.

In this report and earlier ones, we showed that a radar wind sensor (RAWS) is a practical adjunct to a laser wind sensor. The accuracies that can be achieved with the RAWS for entirely cloudy 66-km-square cells and 132-km-square cells are adequate for global atmospheric modeling, at least for the regions where vertical motion is negligible.

When vertical motion is present in rain, we estimate it from the radar echo strength, its relation to rain rate, and the relation between rain rate and fall speed. Such estimates may have significant errors that would dilute the predicted accuracy. Nevertheless, the combined radar and laser sensors should be able to determine the winds at most altitudes even in areas where rain is present. The number of points that would need to be discarded would be small and confined

to the lower altitudes except in strong convective systems. Reducing the number of points used in a large cell by a small fraction will not significantly increase the errors.

As the time approaches for consideration of actual flight systems, it is essential that the radar and laser subsystems be considered together as a total system. If this is done, the scan and shot patterns can be coordinated properly, and the data processing can be common from the point where individual point measurements of Doppler are produced from each subsystem.

# References


[1] R. J. Curran, Ed., *Earth Observation System Instrument Panel Report: LAWS Laser Atmospheric Wind Sounder*, vol. IIg, NASA, Washington DC, 1987.

[2] W. Xin, "A Satellite-Based Radar Wind Sounder," Ph.D. dissertation, Univ. of Kansas, 1990.

[3] R. K. Moore, et al., "A Satellite-Borne Radar Wind Sensor (RAWS)," *Digest IGARSS'92*, Houston, pp. 999-1001, 1992.

[4] M. A. Stuart and R. K. Moore, "Satellite-Based Radar Wind Sounder (RAWS) Optimal Frequency Study," *Digest IGARSS'93*, Tokyo, Japan, pp. 215-217, 1993.

[5] M. A. Stuart, "Radar Sensitivity and Antenna Scan Pattern Study for a Satellite-Based Radar Wind Sounder (RAWS)," M.S. Thesis, Univ. of Kansas, 1992.

[6] S. R. Pallikala and R. K. Moore, "Use of Radar Wind Sensor to Determine Vertical Drop Speed for RAWS," RSL Technical Report 10240-1, Radar System and Remote Sensing Laboratory, Univ. of Kansas, May 1994.

[7] S. R. Pallikala and R. K. Moore, "A Combined IR-Microwave Spaceborne Cloud Profiler," RSL Technical Report 10240-2, Radar System and Remote Sensing Laboratory, Univ. of Kansas, May 1994.

[8] R. J. Doviak and D. S. Zrnic, "Doppler Radar and Weather Observations," Academic Press, New York, 1984.

# CRINC